




RESEARCH ARTICLE

Pain behavior and phenotype in a modified anterior lumbar disc puncture mouse model

Yuming Huang^{1,2,3}  | Linchuan Lei^{1,2,4} | Jian Zhu^{1,2,3} | Jinjian Zheng^{1,2,3} | Zemin Li^{1,2,3} | Hua Wang^{1,2,3} | Jianru Wang^{1,2}  | Zhaomin Zheng^{1,2,3} 

¹Department of Spine Surgery, The First Affiliated Hospital of Sun Yat-sen University, Guangzhou, China

²Sun Yan Sen University, Pain Research Center, Guangzhou, China

³Guangdong Province Key Laboratory of Orthopaedics and Traumatology, Guangzhou, China

⁴Laboratory of General Surgery, The First Affiliated Hospital, Sun Yat-sen University, Guangzhou, China

Correspondence

Jianru Wang and Zhaomin Zheng,
58, Zhongshan 2nd Road, Guangzhou
510080, China.

Email: wangjru@mail.sysu.edu.cn and
zhzhaom@mail.sysu.edu.cn

Funding information

National Natural Science Foundation of China,
Grant/Award Numbers: 81972098, 82072490

Abstract

Background: An experimental study was performed to improve the anterior approach model of intervertebral disc degeneration (IVDD).

Objective: The aims of this study were to investigate the anterior approach model of IVDD for the cause of death, phenotypes, and underlying mechanisms of low back pain in mice.

Method: In this study, we conducted an anterior puncture procedure on a cohort of 300 C57BL/6J mice that were 8 weeks old. Our investigation focused on exploring the causes of death in the study population ($n = 300$) and assessing the time-course changes in various parameters, including radiographical, histological, immunofluorescence, and immunohistochemistry analyses ($n = 10$). Additionally, we conducted behavioral assessments on a subset of the animals ($n = 30$).

Results: Transverse vertebral artery rupture is a major factor in surgical death. Radiographical analyses showed that the hydration of the nucleus pulposus began to decrease at 2 weeks after puncture and obviously disappeared over 4 weeks. 3D-CT showed that disc height was significantly decreased at 4 weeks. Osteophyte at the anterior vertebral rims was observed at 2 weeks after the puncture. As the time course increased, histological analyses showed progressive disruption of the destruction of the extracellular matrix and increased secretion of inflammatory cytokines and apoptosis. Behavioral signs of low back pain were increased between the puncture and sham groups at 4 weeks.

Conclusion: The improvement of anterior intervertebral disc approach model in mice will be useful to investigate underlying mechanisms and potential therapeutic strategies for behavior and phenotypes. Furthermore, the application of vibrational pretreatment can be used to increase the sensitivity of axial back pain in the model,

Yuming Huang, Linchuan Lei, and Jian Zhu authors contributed equally to this work.

This is an open access article under the terms of the [Creative Commons Attribution-NonCommercial-NoDerivs](https://creativecommons.org/licenses/by-nc-nd/4.0/) License, which permits use and distribution in any medium, provided the original work is properly cited, the use is non-commercial and no modifications or adaptations are made.

© 2023 The Authors. *JOR Spine* published by Wiley Periodicals LLC on behalf of Orthopaedic Research Society.

thereby providing researchers with a reliable method for measuring this critical phenotype.

KEYWORDS

animal model, intervertebral disc degeneration, pain behavior, phenotype, vibration

1 | INTRODUCTION

Intervertebral disc degeneration (IVDD) is a major contributor to low back pain (LBP), a leading cause of disability worldwide.¹ The intervertebral disc (IVD) consists of the nucleus pulposus (NP), annulus fibrosus (AF), and cartilaginous endplates (CEPs),² each of which plays a unique role in maintaining disc homeostasis and undergoes distinct pathological changes in degeneration. Various factors, including senescence, inflammatory cytokines, genetics, and environmental factors, can disturb the balance between anabolic and catabolic processes within the disc, leading to degeneration.³ Notably, changes in collagen synthesis in NPCs, including a reduction in type II collagen (Col2) and an increase in type I (Col1) synthesis, occur during disc degeneration, resulting in reduced elasticity and mechanical strength of the tissue.^{3,4} Therefore, ECM remodeling, NPC senescence and death, and inflammatory cytokine presence are the main contributors to IVDD. Appropriate animal models (e.g., rats and mice) of IVDD are critical to understanding its molecular pathophysiology.

There is an increasing use of Knockout mice in IVDD research due to their ability to replicate human genetic mutations and their applicability in gene therapy studies.^{5,6} Therefore, there is a growing interest in developing IVDD models using mice as control animals. Mice and rats have advantages over larger animals, such as cost-effectiveness, ease of handling, and the ability to express quantifiable pain responses. In particular, the mouse model of IVDD has been gaining attention in recent years due to its ability to provide a platform for studying the molecular pathophysiology of IVDD. Among the different methods used to induce IVDD in mice, the most classic puncture model is the posterior approach model.⁷ The second most common approach is the anterior approach,⁸ followed by the lateral approach.⁹ However, due to the small size of the mouse spinal structure, creating the posterior approach model can be time-consuming and challenging to modify.¹⁰ On the other hand, the anterior approach model is associated with high mortality due to the proximity of important vessels and organs.¹¹ Therefore, the development of an effective and minimally invasive mouse model of IVDD is of utmost importance. In this study, we present a modified method that overcomes these challenges and allows for the accurate assessment of pathological changes and behavioral analyses in mice with IVDD.

2 | METHOD

All animal experiments conducted in this study were approved by the Institutional Animal Care and Use Committee of Sun Yat-sen University (Approval No: [2017] 203) and were in accordance with the

approved guidelines. Inbred C57BL/6 mice were obtained from the Animal Center of the First Affiliated Hospital of Sun Yat-sen University and were housed in specific pathogen-free conditions prior to the surgery. Following the operation, the mice were raised in the Animal Experiment Center of the First Affiliated Hospital of Sun Yat-sen University under specific pathogen-free conditions. The mice were maintained in cages at a constant room temperature of $23 \pm 2^\circ\text{C}$, with a humidity level of $50 \pm 10\%$, and subjected to a 12-h light/dark cycle under standard laboratory conditions. They were provided with ad libitum access to food and water and allowed to move freely within their cages while being fed a standard laboratory diet.

2.1 | Surgical procedure

The mouse was positioned in the supine position on the operating table, and the entire ventral abdomen was meticulously prepared by shaving and cleaning with 70% ethanol in double distilled water. Subsequently, a 0.5 cm midline ventral longitudinal incision was made on the skin to expose the white line of the peritoneum. Gentle manipulation of the gut and omentum majus to the right side of the abdominal cavity allowed exposure of the safety triangle area (the inferior margins of the left kidney, spine, and bladder) (Figure S1A). The psoas major muscle bundle, observed converging upward, in an oblique manner, was identified on the medial side of the genitofemoral nerve (Figure S1B). Subsequently, the midline connective tissue was carefully separated using smooth clips to allow visualization of the left psoas major muscle bundles and the position of the IVD (Figure S1C). During the procedure, special care was taken to avoid damage to the transverse vertebral artery (Figure S1D). The ventral aspect of the IVD was visualized through a slow and single penetration with a 27 G limited depth needle in the case of an injured animal or left undisturbed in a sham animal (Video S1).

Following the procedure, the internal organs were carefully restored, and the peritoneum was sutured with 4-0-coated Vicryl sutures. The skin incision was closed with a 4-0 suture, and the animals were closely monitored while kept warm until full recovery from anesthesia. Thereafter, the animals were monitored daily for 7 consecutive days and once a week thereafter.

2.2 | Immunohistochemistry and histopathologic analysis

Tissue specimens were embedded in paraffin and cut into 5- μm sections. We used coronal sections, with one section for each staining

method. Subsequently, the sections were deparaffinized and rehydrated, followed by hematoxylin and eosin (H&E) staining to evaluate general structures and Safranin-O staining to evaluate Cartilage, Cytoplasm, and nucleus. The sections were then blocked with 3% hydrogen peroxide and 5% normal goat serum and incubated with primary antibodies against anti-p21 and anti-p16. Afterward, the sections were incubated with a secondary antibody and developed with DAB solution. Hematoxylin was used for nuclear staining, and eosin was used for cytoplasm staining. Finally, the sections were observed and imaged under an Olympus BX63 microscope and a polarized microscope (Leica) at magnifications of 10 \times , 50 \times , and 400 \times . The expression of p21⁺ and p16⁺ cells in the IVD samples was quantified using ImageJ software (National Institutes of Health, Bethesda, MD, USA). The histologic scores were assessed as previously described.¹²

2.3 | TUNEL staining

TUNEL staining according to the manufacturer's protocol (G1507 Servicebio, China). the sections were deparaffinized and rehydrated, soaked in 0.1 mM citric acid buffer, and the washed with DD water. The sections were rapidly cooled down by addition of 0.1 M Tris-HCl (containing 3% BSA and 20% calf serum). The Recombinant TdT enzyme was dripped onto the sections, and the samples were incubated in a wet box at 37°C for 1 h. soaked in 0.1 mM citric acid buffer, and the washed with water. streptavidin-HRP was dripped onto the sections, and then developed with DAB solution. Finally, the sections were observed and imaged under an Olympus BX63 microscope and polarized microscope (Leica) at 10 \times , 50 \times , and 400 \times magnifications. Positive cells were stained brown.

2.4 | Immunofluorescence

The disc tissues embedded in paraffin were sectioned and deparaffinized in xylene, followed by dehydration in isopropanol dilutions. tissues were then incubated with antibodies: anti-Col1 (1: 100, ab243739, Abcam), anti-Col2 (1:100, #14796, Cell Signaling Technology), anti-ADAMST4, anti-IL-1 β , anti-TNF- α and anti-IL-6, either overnight at 4°C, or 2 h at room temperature. The samples were washed 3 times with 0.1% PBST, and then incubated with anti-mouse/rabbit Alexa 555/594-conjugated second antibody for 2 h at room temperature. The samples were washed again, and the DNA was stained with DAPI (6 μ L DAPI in 100 μ L PBS) for 0.5 h at room temperature. Wash samples and digital images were obtained using a confocal laser scanning microscope (Leica), according to the manufacturer's instructions.

2.5 | von Frey test

To evaluate radiating leg pain, hind paw withdrawal responses to von Frey filament stimulation were utilized. In brief, after allowing mice to acclimate for 15 min in individual wire mesh cages, von Frey filaments

were applied in an ascending sequence, starting with the 1.4 g filament, to the plantar surface of each hind paw until the filament buckled slightly. If no response was elicited after 3 s, the next filament with increasing force was applied until hind paw withdrawal was observed. Conversely, if a hind paw withdrawal response occurred within 3 s, the next filament of decreasing force was used. Each ipsilateral and contralateral hind paw was measured three times with a 5-min interval between consecutive measurements, and the mean withdrawal force was determined by selecting the lower readings group. Animals that did not respond to any of the von Frey filaments were assigned a score of 4 g.

2.6 | Thermal radiation test

Thermal hyperalgesia was assessed by measuring the hind paw withdrawal latency in mice. Prior to the assessment, mice were allowed to acclimate to the tempered (29°C) glass surface of the plantar cage, and major grooming activities were ceased. A radiant heat source was positioned under the plantar surface of the hind paw with a time limit of 30 s to avoid skin damage. The withdrawal latency for both hind paws were determined from the average of three separate trials, conducted at 5 min intervals, and the latency time was determined from the lower readings group. The presence of clear paw withdrawal, shaking or licking after heat stimulation were considered nociceptive-like responses.

2.7 | Cold plate test

To assess cold sensitivity, the cold plate test was performed. Mice were placed on a cold plate (10°C) with one hind paw and the latency to withdrawal or paw licking was measured. The test was repeated three times for each paw with a 10-min interval between measurements, and the average of the three assays was used as the individual threshold for each paw. Latency time was determined using the group with the lowest readings.

2.8 | Vibration pre-treatment

Prior to pressure algometry and behavioral testing, mice were exposed to 15 min of axial whole-body vibration with free posture at a frequency of 45 Hz, using a previously reported vibration platform.

2.9 | Pressure algometer test

Prior to pressure algometry, the mouse was placed prone on a warm pad and allowed to acclimate for 5 min. The device tip was then pressed directly on the dorsal skin over the punctured discs (L4/L5, L5/L6). Mechanical force was applied at a rate of approximately 100 g/s on the dorsum at lumbar levels L4/L5 to assess the pressure

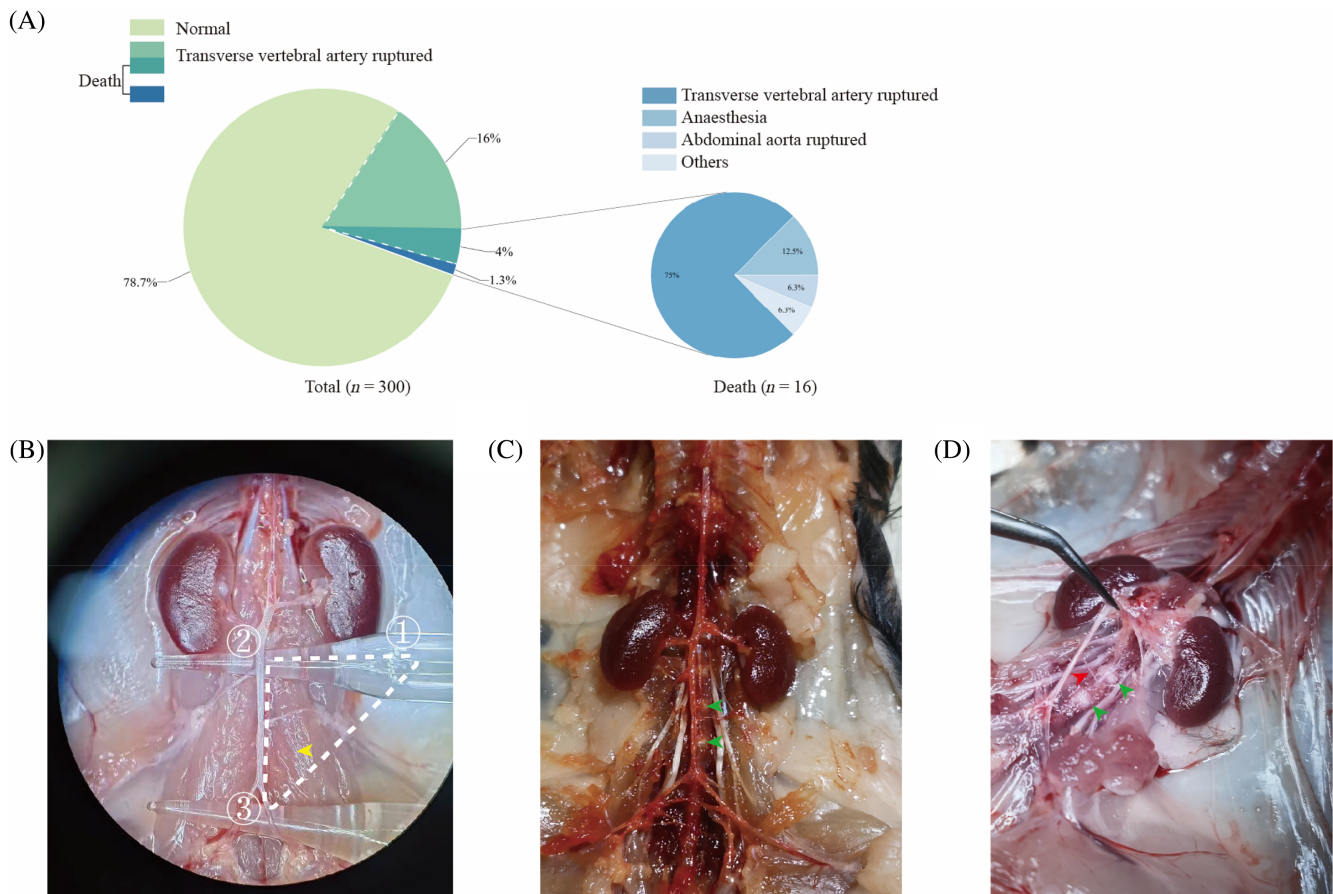


FIGURE 1 Transverse vertebral artery ruptured is a major factor of surgical death. (A) Pie chart illustrates the causes of death in mice. (B) Safety triangle area, ①: inferior margins of left kidney; ②: spine; ③: bladder. Glass rod indicated the abdominal aorta, yellow arrow indicated the genitofemoral nerve. (C) Regional anatomy of intervertebral disc section. Green arrow indicated the intervertebral disc. (D) The transverse vertebral artery is a branch of the abdominal aorta. Red arrow indicated the transverse vertebral artery; green arrow indicated the intervertebral disc.

algometry thresholds (PATs) that elicited audible vocalization or discomfort. To prevent tissue trauma, a cut-off force of 500 g was used. The baseline PATs for L4/L5 were calculated as the mean of three readings for each region, with consecutive measurements separated by at least 5-min intervals.

2.10 | Behavioral testing

In this experiment, mice were placed in a transparent acrylic box, and two specific behaviors (grooming and “wet dog shake”) were evaluated as signs of pain according to previous literature.^{13–15} The behavior of each mouse was recorded for 10 min using a timer. When an animal displayed a behavior, the corresponding button was pressed to start recording the duration of that behavior. “Wet dog shake” (WDS) is a behavior similar to a wet dog shaking its body to get rid of water from its fur. This behavior was recorded as the number of occurrences during the 10-min observation period and was counted using a specially designed “count” button in parallel with the process of recording other behaviors.

3 | RESULTS

3.1 | Transverse vertebral artery rupture is a major factor of surgical death

Prior to conducting this study, we observed a vascular structure crossing the anterior aspect of the vertebrae. Although its rupture did not interfere with the puncture procedure, it increased intraoperative bleeding in mice. Therefore, we hypothesized that rupture of this artery may lead to perioperative mortality in mice. Our statistical data revealed that among the 300 mice subjected to the surgical procedure, 20% showed rupture of the vertebral artery, and in those with vertebral artery rupture, the mortality rate was 20%, accounting for 75% of the total mortality (Figure 1A).

Anatomical findings demonstrated that the safety triangle area was an ideal surgical site, with only one genitofemoral nerve passing through the region (Figure 1B). The abdominal aorta wrapped around the surrounding connective tissue and tended to incline toward the right side of the trunk (Figure 1C). Subsequently, we injected a filling agent into the artery to visualize its branching pattern. Under the

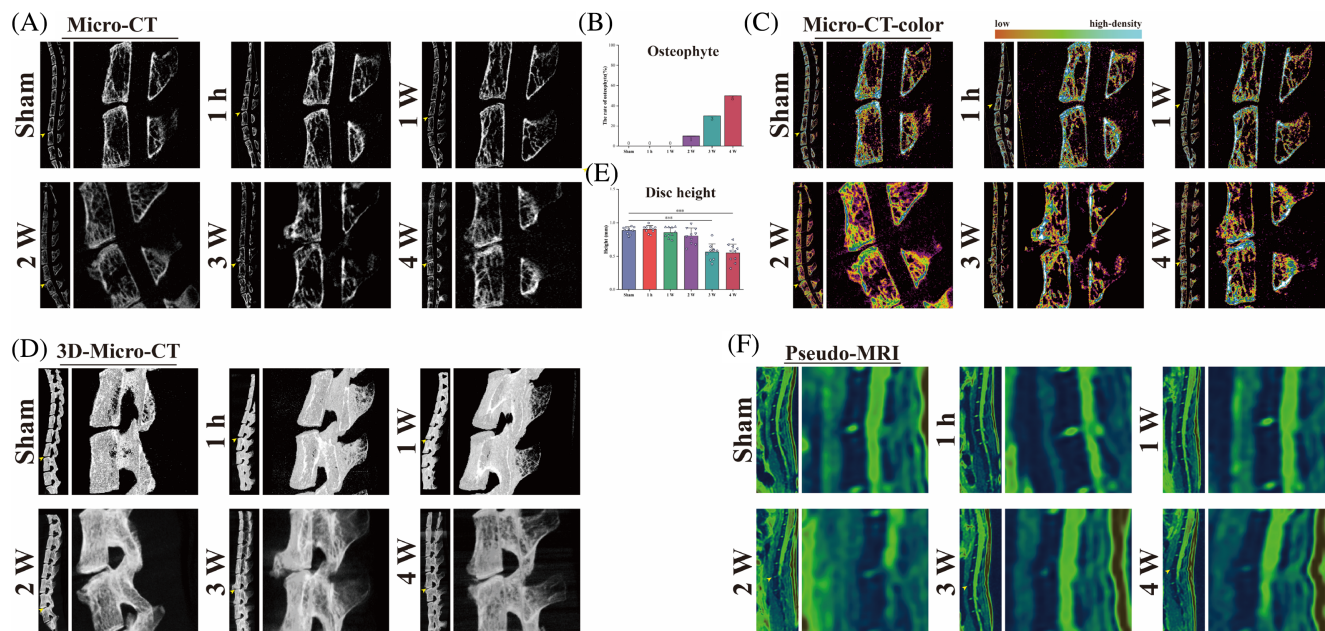


FIGURE 2 Effect of IVD punctured on the radiographic changes. (A and B) Micro-CT images of Injury levels at 2-weeks following puncture reveals the Osteophytes. At the 4-weeks following puncture, Osteophytes occurs in the adjacent vertebrae. (C) Micro-CT-color reveals Osteophytes properties is cancellous bone at 2-weeks and cortical bone at 4-weeks. The indicator card shows the color change from cancellous bone to cortical bone. (D and E) Three-dimensional micro-CT (3D micro-CT) shows 4 weeks after punctured, the disc height was worse preserved, when compared to 3 weeks. (F) Pseudo-MRI shows that 2 weeks after punctured, the NP tissues degenerates and significantly decreases at 4 weeks. the NP is bright green, the AF is dark green, and the vertebrae is black. $n = 10$; * $p < 0.05$. ** $p < 0.01$. *** $p < 0.001$. Statistical comparison was conducted using one-way ANOVA, followed by Student's *t*-test. Each dot represents the mean value of three technical replicates. Each dot represents the mean value of three technical replicates.

microscope, transverse vertebral artery was observed to be a branch of the abdominal aorta (Figure 1D).

3.2 | Time course of radiographic changes

Micro-CT imaging revealed that bone remodeling and osteophyte formation were observed at the anterior edge of the punctured vertebrae as early as 2 weeks post-surgery (Figure 2A). The incidence of osteophyte formation significantly increased over time, with 50% of punctured vertebrae showing osteophyte formation by the 4th week post-surgery (Figure 2B). Micro-CT color images of the vertebral sagittal plane demonstrated the density changes of osteophytes, which shifted from trabecular bone toward higher-density cortical bone (Figure 2C). In addition, we calculated the intervertebral disc height from the 3D-CT images and found a gradual reduction over time (Figure 2D). There was a significant difference at the 3-week time point compared to the previous time points, and a clear decreasing trend at the 4-week time point (Figure 2E).

T2-weighted MRI signal intensity is commonly used to evaluate intervertebral disc health, and we used pseudocolor, which is different from T2-weighted MRI (black and white). Pseudocolor has a color difference that is more recognizable to the human eye (Figure 2F). Pfirrmann analysis showed a significant increase in degeneration grade at 3 weeks post-surgery, and all samples showed IVDD at 4 weeks post-surgery.

3.3 | Anterior approach model changes the histopathology and ECM

Histological staining with H&E, S&O demonstrated that normal IVDs possess an intact AF with a distinct border between the AF and NP. As time progressed, the NP gradually decreased and collapsed, while the number of chondrocyte-like cells increased and the proteoglycan content decreased. Especially during the 3rd to 4th week post-surgery, the NPCs content significantly decreased, the border diminished, the AF tissue became thinner and more disorganized, and the height between the upper and lower endplates decreased noticeably. In the S&O staining, the IVD cells were covered by proliferative chondrocytes that replaced the blue-colored osteoblasts (Figure 3A).

Aggrecan and Col are two major components of IVD extracellular matrix (ECM), which are cleaved and regulated by ADAMTS (A Disintegrin and Metalloproteinase with Thrombospondin motifs).^{16,17} Therefore, we selected ADAMTS4, Col1, and Col2 for multiple immunofluorescence staining. In normal IVDs, Col2 exists in the inner ring of the NP and AF. As time elapsed, Col2 initially disappeared from the inner edge of the AF at postoperative week 1, and then it expanded from the outer periphery of the NP to the AF. Second, we found that the expression positions of Col1 and ADAMTS4 were the same (Figure 3B). In NP tissue, the expression of Col1 and ADAMTS4 gradually increased, while Col2 was the opposite (Figure 3C-E). In AF tissue, the expression of ADAMTS4

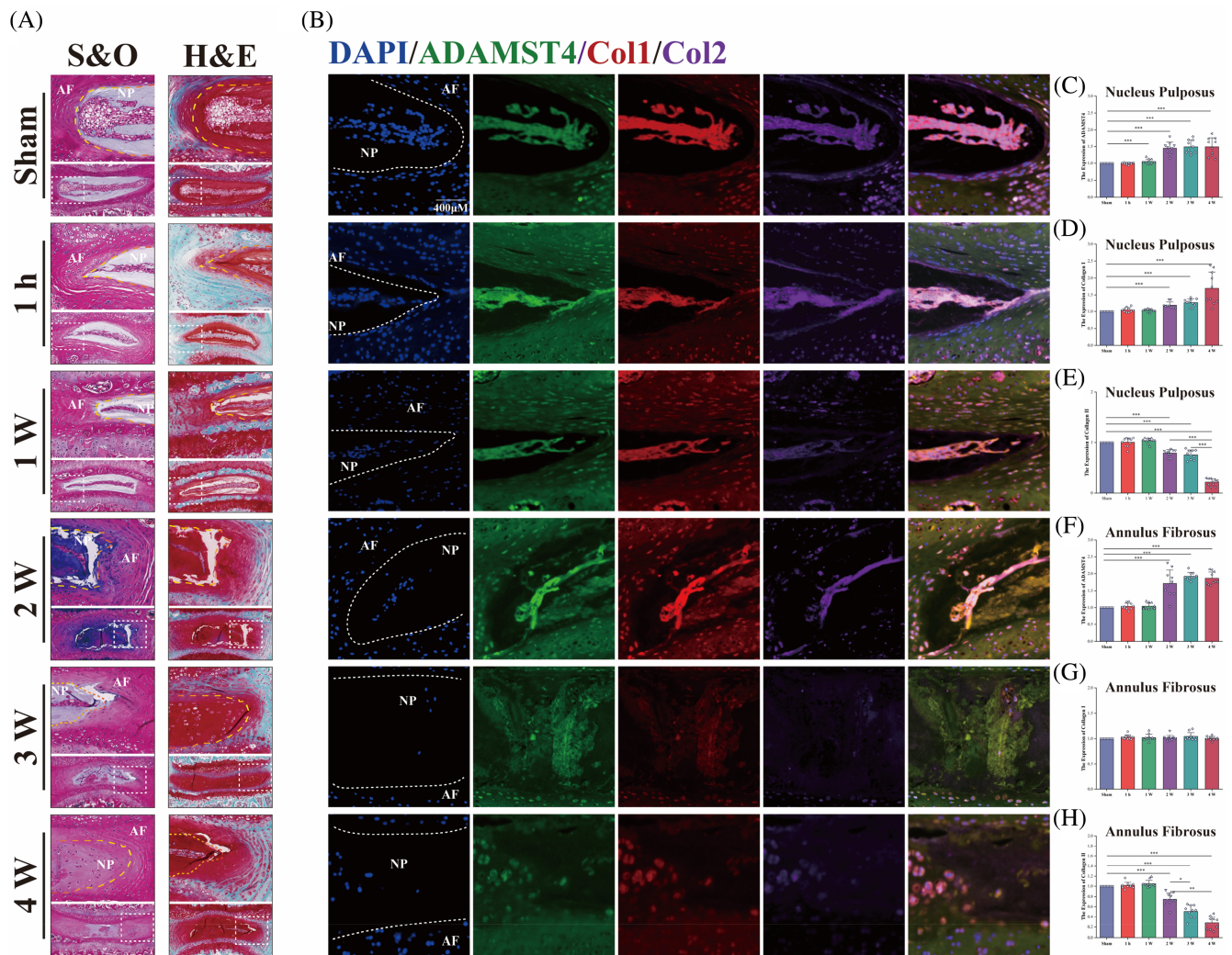


FIGURE 3 Anterior approach model changes the histopathology and ECM. (A) Hematoxylin & Eosin and Safranin-O & FAST Green staining, Magnified intervertebral disc images (bottom). from 2-weeks after punctured, the boundary between the nucleus pulposus and the annulus fibrosus gradually becomes unclear. (B) Representative immunofluorescence staining for ADAMST4 (green), Collagen I (red), Collagen II (purple) and DAPI (blue). (C) The expression of ADAMST4 in Nucleus Pulposus tissues, from 2-weeks after punctured, ADMAST4 is significantly increased compared to the Sham group. (D) The expression of Collagen I in Nucleus Pulposus tissues, any group of Collagen I is not change compared to the Sham group. (E) The expression of Collagen II in Nucleus Pulposus tissues, from 2-weeks after punctured, Collagen II is significantly decreased compared to the Sham group. Subsequently, Collagen II decreased significantly every week. (F) The expression of ADAMST4 in Annulus Fibrosus tissues, from 2-weeks after punctured, ADMAST4 is significantly increased compared to the Sham group. (G) The expression of Collagen I in Annulus Fibrosus tissues, from 2-weeks after punctured, ADMAST4 is significantly increased compared to the Sham group. (H) The expression of Collagen II in Annulus Fibrosus tissues, from 2-weeks after punctured, Collagen II is significantly decreased compared to the Sham group. Subsequently, Collagen II decreased significantly every week. Scale bar: 400 μm and 200 μm . $n = 10$; * $p < 0.05$. ** $p < 0.01$. *** $p < 0.001$. Statistical comparison was conducted using one-way ANOVA, followed by Student's t -test. Each dot represents the mean value of three technical replicates. Each dot represents the mean value of three technical replicates.

gradually increased, while Col2 was the opposite, and the expression of Col1 did not change (Figure 3F-H).

3.4 | Anterior approach model increases the secretion of inflammatory cytokines

IL-6 is known to enhance the catabolic effects of IL-1 β and TNF- α on NPCs.¹⁸ Therefore, we examined the expression of IL-1 β , TNF-

α , and IL-6 in the IVD. At all-time points, the expression positions of TNF- α and IL-6 were the same, prominently expressed in the ECM surrounding the NP tissue, especially in severely degenerated IVDs, while the expression of IL-1 β was closer to the cells. The boundary between them was no longer apparent during degeneration (Figure 4A). The expression of IL-1 β , TNF- α , and IL-6 gradually increased over time in the IVD, with a significant increase observed starting from 3 weeks postoperatively (Figure 4B-G).

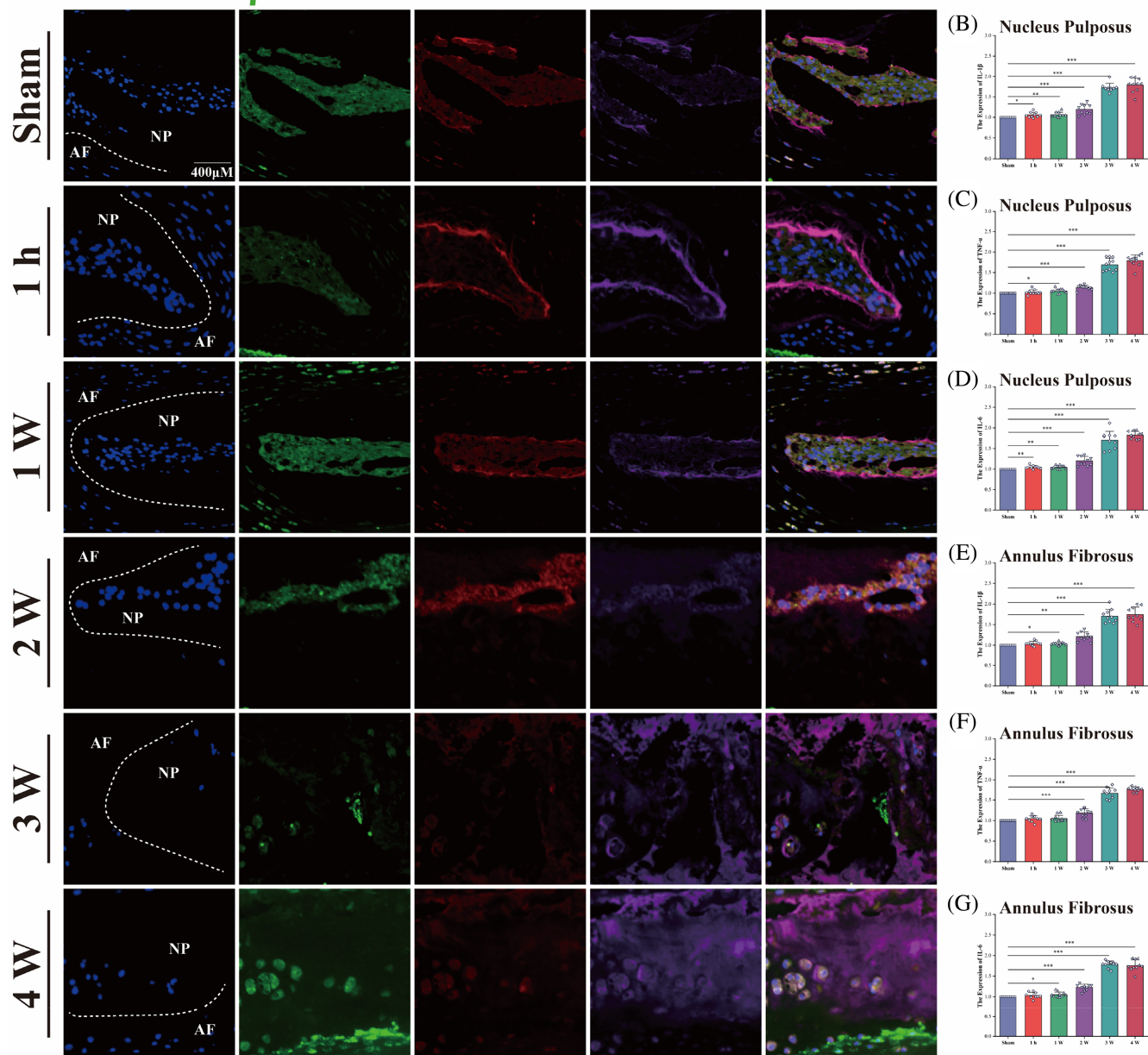
(A) DAPI/IL-1 β /TNF- α /IL-6

FIGURE 4 Anterior approach model increases the secretion of inflammatory cytokines. (A) Representative immunofluorescence staining for IL-1 β (green), TNF- α (red), IL-6 (purple), and DAPI (blue). (B) The expression of IL-1 β in Nucleus Pulposus tissues, from 1-week after punctured, IL-1 β is significantly increased compared to the Sham group. (C) The expression of TNF- α in Nucleus Pulposus tissues, from 1-week after punctured, TNF- α is significantly increased compared to the Sham group. (D) The expression of IL-6 in Nucleus Pulposus tissues, from 1-week after punctured, IL-6 is significantly increased compared to the Sham group. (E) The expression of IL-1 β in Annulus Fibrosus tissues, from 1-h after punctured, IL-1 β is significantly increased compared to the Sham group. (F) The expression of TNF- α in Annulus Fibrosus tissues, from 1-week after punctured, TNF- α is significantly increased compared to the Sham group. (G) The expression of IL-6 in Annulus Fibrosus tissues, from 1-h after punctured, IL-6 is significantly increased compared to the Sham group. Scale bar: 400 μ m. $n = 10$; * $p < 0.05$. ** $p < 0.01$. *** $p < 0.001$. Statistical comparison was conducted using one-way ANOVA, followed by Student's t -test. Each dot represents the mean value of three technical replicates. Each dot represents the mean value of three technical replicates.

3.5 | Anterior puncture increases early NPC apoptosis rather than senescence

During the process of IVDD, cell apoptosis first occurs in the NP tissue [100]. We analyzed the apoptosis of NPCs using TUNEL staining.

Cell apoptosis occurred 1 h after puncture and significantly increased in the first week after surgery. As time passed, the number of NPCs gradually decreased, but the apoptosis rate of NPCs remained above 80%, and at 3 weeks post-surgery, 90% of NPCs underwent apoptosis, which was consistent with AF (Figure 5A-C).

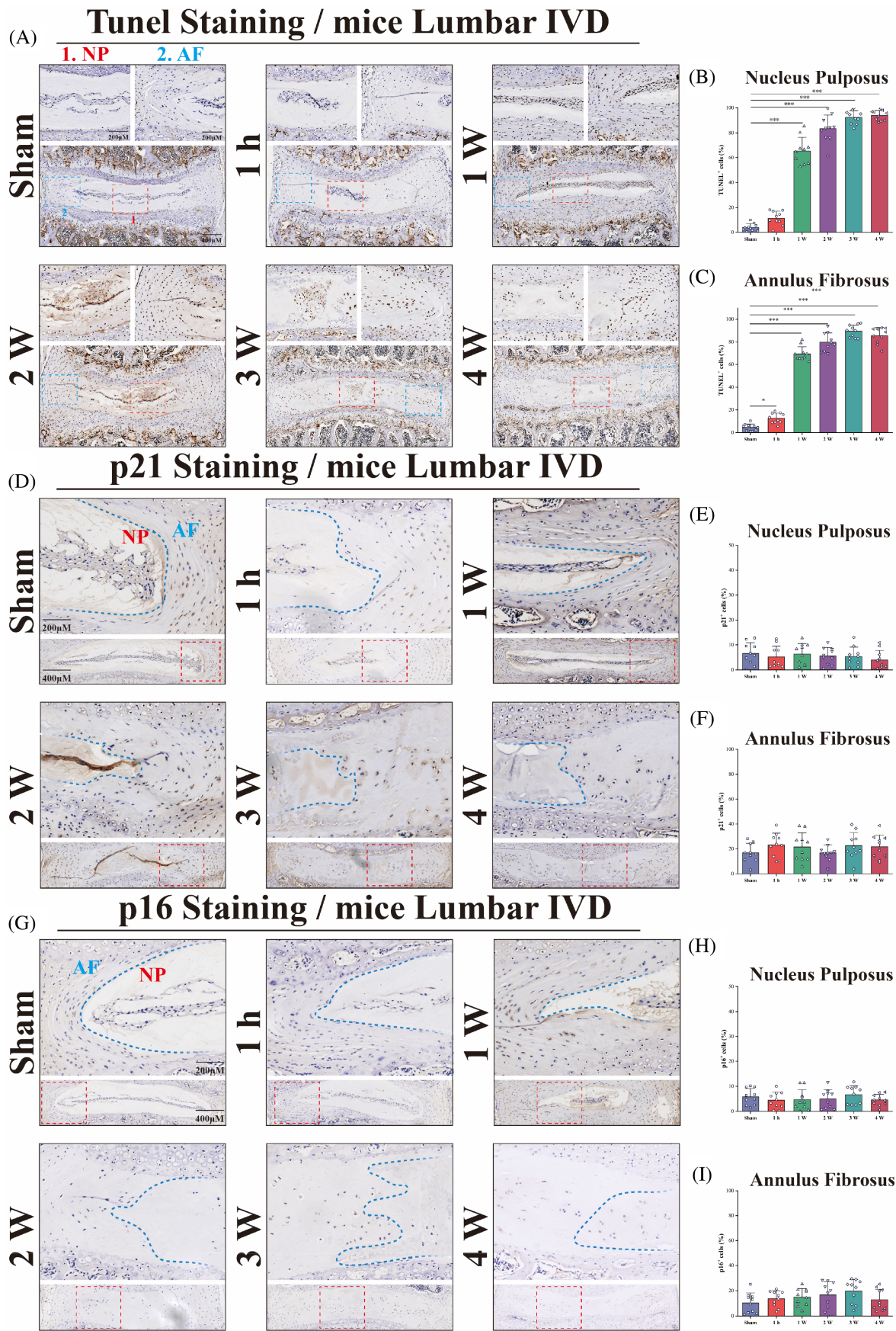
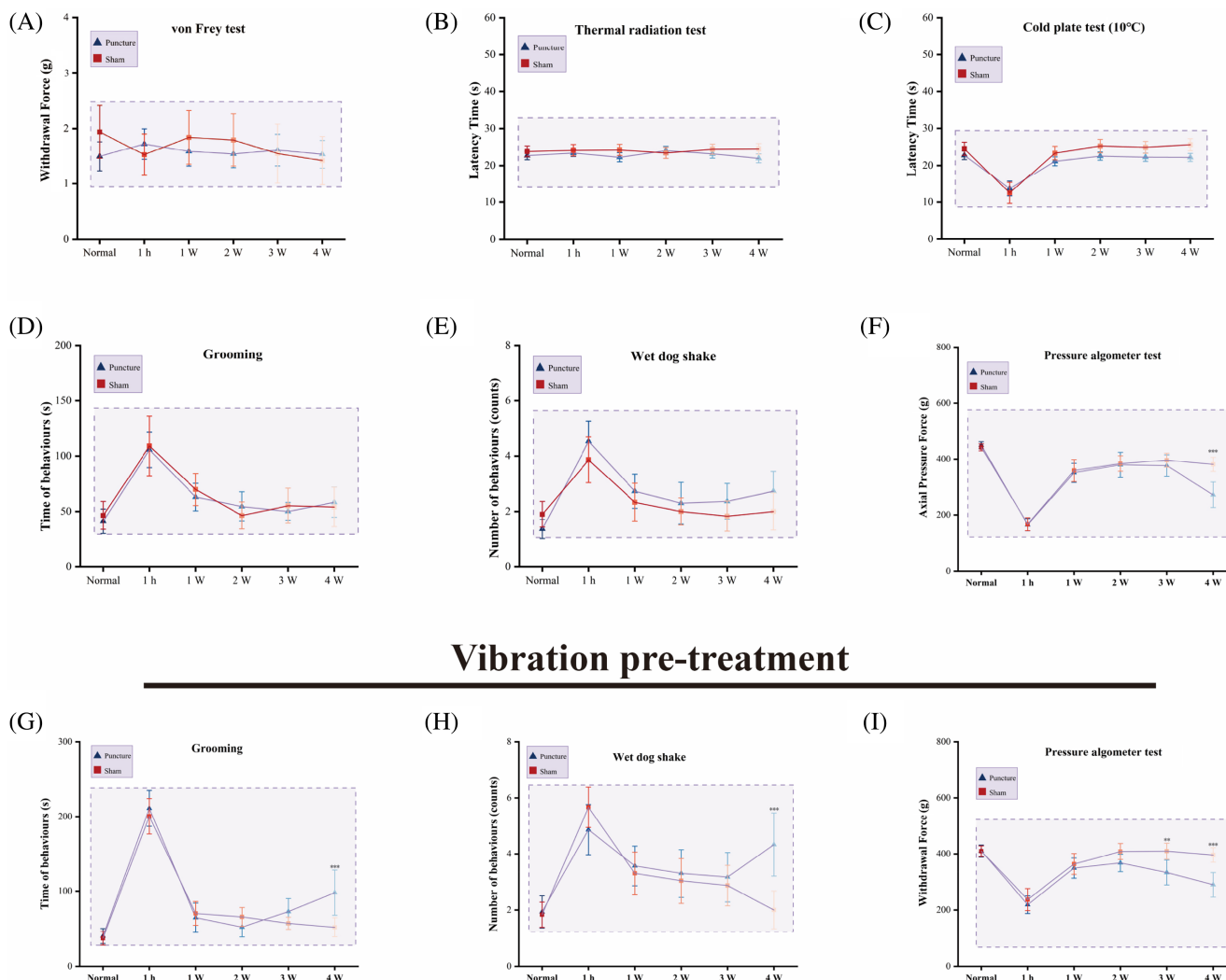


FIGURE 5 Legend on next page.



Vibration pre-treatment

FIGURE 6 Evaluation of behavioral measures after anterior puncture. (A) The von Frey test was employed to compare the puncture group with the sham group at various time points, and no significant differences were observed. (B) The thermal radiation test was utilized to compare the puncture group with the sham group at various time points, and no significant differences were observed. (C) The cold plate test was utilized to compare the puncture group with the sham group at various time points, and no significant differences were observed. (D and E) Spontaneous behaviors were used to compare the puncture group with the sham group at various time points, and no significant differences were observed. (F) The pressure algometer test was employed to compare the puncture group with the sham group, and significant differences were observed at the postoperative 4th week. (G and H) Following vibration pre-treatment, spontaneous behaviors were utilized to compare the puncture group with the sham group, and significant differences were observed at the postoperative 4th week. (I) Following vibration pre-treatment, the pressure algometer test was employed to compare the puncture group with the sham group, and significant differences were observed from the postoperative 3rd week. $n = 30$; $*p < 0.05$. $**p < 0.01$. $***p < 0.001$. Statistical comparison was conducted using one-way ANOVA, followed by Student's t-test. Each dot represents the mean value of three technical replicates.

FIGURE 5 Anterior puncture increases early NPCs apoptosis rather than senescence. Nucleus Pulposus (NP) tissues at red area (left), Annulus Fibrosus (AF) tissues at blue area (right). (A–C) Representative immunohistochemical images of TUNEL staining show a significant increase in the rate of TUNEL⁺ cells in the Nucleus Pulposus and Annulus Fibrosus tissues starting from 1 week post-surgery. (D–F) Representative immunohistochemical images of p21 staining reveal no significant changes in the rate of p21⁺ cells in both Nucleus Pulposus and Annulus Fibrosus tissues. (G–I) Representative immunohistochemical images of p16 staining reveal no significant changes in the rate of p16⁺ cells in both Nucleus Pulposus and Annulus Fibrosus tissues. Scale bar: 400 and 200 μm . $n = 10$; $*p < 0.05$. $**p < 0.01$. $***p < 0.001$. Statistical comparison was conducted using one-way ANOVA, followed by Student's t-test. Each dot represents the mean value of three technical replicates.

p16 and p21 are typical markers of senescence.^{19,20} Immunohistochemistry staining showed that the expression of p21 and p16 did not change within 4 weeks after puncture (Figure 5D-I).

3.6 | Evaluation of behavioral measures after anterior puncture

Axial low back pain and radiating leg pain are common symptoms of IVDD, but they are caused by different mechanisms.²¹ von Frey testing showed no significant differences between the puncture and sham surgery groups within 4 weeks, and the differences observed preoperatively and 1 h after surgery may be due to anesthesia (Figure 6A). Additionally, we conducted thermal sensitivity tests, which showed no differences between the puncture and sham surgery groups within 4 weeks (Figure 6B,C). Our results suggest that the anterior approach puncture did not induce radiating leg pain in mice.

Increasing the sensitivity for detecting LBP is challenging, we utilized the observation of spontaneous behavior method to capture behavioral responses related to LBP.¹³ Additionally, we employed a pressure algometer test to quantify pain sensitivity specifically associated with LBP. Within 4 weeks after surgery, there were no significant differences between the puncture and sham surgery groups in the spontaneous behavior test (Figure 6D,E). The pressure algometer test showed no significant differences between the two groups within 3 weeks after surgery, but in the fourth week, significant differences between the puncture and sham surgery groups were observed (Figure 6F). Furthermore, after using vibration pre-treatment, there were no significant differences in the spontaneous behavior test between the puncture and sham surgery groups within 3 weeks after surgery, but in the fourth week, the puncture group showed a significant increase (Figure 6G,H). Similarly, in the mouse pressure algometer test, significant differences were observed between the puncture and pressure pain groups starting from the third week after surgery (Figure 6I). We conclude that anterior approach puncture can induce LBP in mice, and vibration pre-treatment can increase the sensitivity for detecting LBP.

4 | DISCUSSION

The establishment of a suitable and effective animal model is of utmost importance for investigating the pathogenesis of diseases. Among them, the mouse puncture model serves as an excellent control group for knockout mice. Although some studies have reported the feasibility of an anterior approach, the lack of documentation of the cause of death and surgical video, as well as the need to modify the visceral exposure and complex surgical techniques,^{8,11,22} call for improvements. In this study, we present a highly efficient IVDD model that minimizes the risk of mortality while validating different IVDD phenotypes in correspondence with the model. The significance of this model lies in its capacity to facilitate the exploration of the underlying mechanisms and potential therapeutic targets for IVDD.

4.1 | Anatomical characteristics of the current model

We have also identified a potentially significant cause of major bleeding during the anterior approach surgery, which is the transverse vertebral artery. In our experiments, we observed that the transverse vertebral artery was more susceptible to accidental injury during surgery compared to the abdominal aorta. Although the use of colored infusion agents has been reported to aid in visualizing the puncture site and reducing the risk of nerve and muscle injury, it is not effective in visualizing smaller arteries such as the transverse process artery.¹¹

We found that approximately 20% of anterior approach procedures resulted in transverse vertebral artery injury. Moreover, in those cases where the artery was damaged, approximately 20% of the mice died during the perioperative period, accounting for 75% of all deaths. Therefore, identifying the cause of death is crucial for reducing the mortality rate associated with anterior approach modeling. To avoid damaging the transverse vertebral artery and reducing the mortality rate of mice, we defined a “safe triangle area” bounded by the lower edge of the left kidney, the upper edge of the bladder, and the spinal midline. We found that exploration within this region under a microscope could avoid major blood vessels and nerve bundles such as the abdominal aorta, while also avoiding the sciatic nerve.

The bilateral lumbar muscles converge at the midline of the spinal vertebrae, and under the microscope, the muscle bundles can be observed running diagonally upward. The anatomic location of the intervertebral disc can be easily located along the direction of the muscle bundles. The safe triangle region typically contains two intervertebral discs (L3-4 and L4-5). Based on our analysis, the ratio of puncturing these two intervertebral discs is approximately 1:2. This also implies that a more precise selection of corresponding spinal segments can be made during modeling.

4.2 | Radiographic characteristics of IVDD

In order to accurately diagnose IVDD, imaging modalities such as x-ray, CT, and MRI are commonly used in both human and animal studies. Currently, the disappearance of NP hydration is considered a specific phenotype of IVDD. However, using MRI in mice presents certain challenges. First, a magnetic field strength of at least 3.0 T is required to achieve clear imaging results.²³ In this study, we employed a pseudocolor method to visualize the NP. While this technique has been used in humans for some time, it has not been widely studied in mice.

Second, we found that the height of the intervertebral disc is closely correlated with the number of NPCs. To determine the height of the intervertebral disc more accurately, we utilized 3D-CT imaging to calculate its volume. This approach provides a more precise method for calculating disc height. However, it is worth noting that in basic research, imaging features are often overlooked. We believe that this

feature should be given greater attention and considered as an important factor in accurately diagnosing IVDD.

4.3 | ECM characteristics of IVDD

Puncture-induced alterations in the AF and NP immediately disrupt the ecological niche. The decrease in NP content over time has been reported in numerous studies.^{24,25} Our investigation revealed that the optimal time for studying IVDD in mice is 3–4 weeks post-surgery, which ensures the presence of NP and incomplete loss of NP cells. In the past, the optimal time for IVDD modeling in rats was reported to be 8 weeks, but this may not be applicable to mice. The time required for modeling IVDD may also differ for different phenotypes. Previous studies have demonstrated a decrease in Col2 in NP tissue during IVDD.^{26,27} In our study, we observed a dynamic process of Col2 degradation in the NP ecological niche after anterior puncture. The degradation began from the inner ring of the AF and gradually spread to the NP tissue surrounding the AF, which may reflect a time-dependent deterioration of the ECM. Furthermore, we found that the expression of Col1 gradually increased in the area surrounding the NP tissue. Our observations suggest that the progression of IVDD in the anterior puncture model involves a complex interplay between the degradation of Col2 and the increased expression of Col1, which may contribute to the abnormal ECM distribution and structural changes in the intervertebral disc. Additionally, ADAMTS4, a known factor involved in ECM degradation, was found to be closely associated with Col1 rather than Col2 during the later stages of IVDD, suggesting a potential role in the synthesis of Col1. Notably, the anterior approach for modeling IVDD in mice caused significant ECM deterioration, mainly in the form of abnormal distribution of Col1 and Col2.

4.4 | Inflammatory cytokines associated with IVDD

The presence and distribution of inflammatory cytokines are known to have a significant impact on NPCs in patients with IVDD.²⁸ In this study, we focused on three key inflammatory cytokines, namely TNF- α , IL-1 β , and IL-6. Interestingly, the distribution of IL-1 β was markedly distinct from that of the other two cytokines, suggesting the involvement of distinct biological pathways. Previous studies have shown that IL-6 can synergize with TNF- α , while IL-1 β only produces a synergistic effect at higher concentrations, which is in line with our findings regarding their respective distributions.^{18,29} In healthy IVDs, TNF- α and IL-6 are mainly distributed in the ECM surrounding the NP tissues, while IL-1 β is localized in NPCs. However, with the progression of IVDD, TNF- α and IL-6 gradually accumulate in NPCs, leading to the blurring of boundaries between the three cytokines. Moreover, we observed a contrasting trend between the levels of IL-6 and Col2, with the former decreasing while the latter increasing, indicating the complex interplay between inflammatory cytokines and the ECM during the pathogenesis of IVDD.

4.5 | Potential mechanisms of apoptosis and senescence

The progression of IVDD is tightly linked to the apoptosis and senescence of IVD cells, which can be triggered by long-term exposure to stress or mechanical injury. Such exposure can lead to the upregulation of apoptosis-inducing factors, including growth arrest and DNA damage, resulting in cell apoptosis and senescence.³⁰ Our investigation demonstrated that apoptosis occurred immediately after surgery, leading to a stabilized TUNEL-positive rate at approximately 80% within 2–4 weeks, indicating that apoptosis is a suitable phenotype for studying IVDD in a relatively short period of time.

Senescence has emerged as an important research topic in recent years,³¹ and p21^{32,33} and p16^{34,35} have been identified as markers of senescence. However, our investigation revealed that the rate of cell senescence was low at 4 weeks in the anterior puncture model, suggesting that this model may not be appropriate for studying the senescence phenotype. Inducing senescence may require a longer time, but the NP tissue may disappear after 4 weeks. Thus, we conclude that the anterior puncture model is not an ideal method for modeling the senescence phenotype in mice.

4.6 | Potential mechanisms underlying behavioral measures

In our study, the focus was to establish a reliable model for LBP. Generally, the assessment of pain in LBP patients involves a physical examination that includes axial and radiating pain, such as the von Frey test and temperature stimuli.^{36,37} Previous animal studies have demonstrated that anterior puncture is not a significant factor in inducing radiating pain,³⁸ which is consistent with our findings. We suggest that rats and mice exhibit a high tolerance for pain, and radiating pain is primarily caused by IVD protrusion or compression of the dorsal root ganglia. However, our puncture did not damage the dorsal root ganglia or cause direct compression, regardless of whether the dorsal root ganglia were stimulated or compressed.

During IVDD, most patients experience axial back pain before radiating leg pain, and the presence of back discomfort is usually associated with IVDD. Detecting axial back pain in animal models is challenging, and it can only be determined through spontaneous behavior and pain-related behavior. Currently, there are no direct methods for measuring back pain. Therefore, we combined previous research and used spontaneous behavior (including grooming and WDS),^{13,39} and pressure algometer test.⁴⁰ At 4 weeks post-surgery, there was a significant difference in pressure algometer test between the two groups of mice, which we believe is related to IVDD. However, there was no difference in spontaneous behavior between the two groups. Increasing the sensitivity of axial back pain is crucial for early detection of IVDD. Therefore, we used vibrational pre-treatment to enhance the sensitivity of axial back pain, which was based on the theory of inducing LBP by vibration in previous studies.^{41,42} Based on

previous research,⁴³ short-term vibration does not worsen IVDD, ensuring the stability of the model. In our study, after vibrational pre-treatment, there was a significant increase in spontaneous behavior in the mice at 4 weeks post-surgery, mainly characterized by an increase in grooming and WDS behavior. Additionally, the pressure algometer test showed a significant difference between the anterior puncture group and the sham group from the third week post-surgery. Thus, we conclude that anterior puncture is a suitable model for studying IVDD and its associated LBP. Vibrational pre-treatment can increase the sensitivity of axial back pain.

The implementation of the anterior approach model in this study demonstrates a substantial reduction in mortality rates during anterior disc modeling in mice, thereby providing a reliable and stable methodology for intervertebral disc research. However, it is important to note that the mouse model presents limitations due to the requirement for microscopic manipulation, whereas rat surgery is comparatively more accessible and associated with minimal tissue damage. Moreover, rats can accommodate larger grafts than mice. Additionally, it should be acknowledged that the puncture model employed in this study only partially replicates the etiology of human lower back pain, specifically focusing on lumbar pain resulting from annular rupture.

In this study, we performed a comprehensive analysis of the suitability of the anterior puncture model for IVDD modeling in mice. While we found this approach to be feasible for most basic research, further exploration is necessary to determine its efficacy in pain-related studies, and alternative surgical approaches, such as the posterior approach, may be worth exploring. The absence of comparative analysis with different approaches is a limitation of this study, and future research should aim to address this issue to better evaluate the effectiveness of the anterior puncture model in IVDD and pain-related research.

5 | CONCLUSION

Improvements to the anterior intervertebral disc approach model in mice have the potential to advance the investigation of underlying mechanisms and potential therapeutic strategies for a range of phenotypes and behavioral manifestations of IVDD. Furthermore, the application of vibrational pre-treatment can be used to increase the sensitivity of axial back pain in the model, thereby providing researchers with a reliable method for measuring this critical phenotype. The identification of such techniques may have significant implications for the development of new therapeutic interventions to manage IVDD and associated LBP.

AUTHOR CONTRIBUTIONS

Yuming Huang, Linchuan Lei, and Jian Zhu draft manuscript and collected data. Zhaomin Zheng and Jianru Wang designed the study. Hua Wang and Zemin Li carried out data analyses. Yuming Huang produced initial draft of manuscript. All authors read and approved final manuscript.

ACKNOWLEDGMENTS

Thanks to some of the instruments provided by the experimental platform of Prof. Cao Kaiyuan of Sun Yat-sen University.

FUNDING INFORMATION

This work was supported by National Natural Science Foundation of China (81972098 [Jianru Wang] and 82072490 [Zhaomin Zheng]).

CONFLICT OF INTEREST STATEMENT

The authors declare no conflicts of interest.

DATA AVAILABILITY STATEMENT

Data available on request from the authors.

ORCID

Yuming Huang  <https://orcid.org/0000-0002-7693-6417>

Jianru Wang  <https://orcid.org/0000-0002-9747-0652>

Zhaomin Zheng  <https://orcid.org/0000-0002-1624-4136>

REFERENCES

- Chiarotto A, Koes BW. Nonspecific low back pain. *N Engl J Med*. 2022;386:1732-1740.
- Lyu FJ, Cheung KM, Zheng Z, Wang H, Sakai D, Leung VY. IVD progenitor cells: a new horizon for understanding disc homeostasis and repair. *Nat Rev Rheumatol*. 2019;15:102-112.
- Raj PP. Intervertebral disc: anatomy-physiology-pathophysiology-treatment. *Pain Pract*. 2008;8:18-44.
- Wagner DR, Lotz JC. Quantifying the contributions of structure to the annulus fibrosus mechanical function using a nonlinear, anisotropic, hyperelastic model. *J Orthop Res*. 2008;26(1675):1675-1676.
- Wang Z, Chen H, Tan Q, et al. Inhibition of aberrant Hif1alpha activation delays intervertebral disc degeneration in adult mice. *Bone Res*. 2022;10:2.
- Bian Q, Ma L, Jain A, et al. Mechanosignaling activation of TGFbeta maintains intervertebral disc homeostasis. *Bone Res*. 2017;5:17008.
- Oichi T, Taniguchi Y, Soma K, et al. A mouse intervertebral disc degeneration model by surgically induced instability. *Spine*. 2018;43:E557-E564.
- Millecamps M, Stone LS. Delayed onset of persistent discogenic axial and radiating pain after a single-level lumbar intervertebral disc injury in mice. *Pain*. 2018;159:1843-1855.
- Walk RE, Moon HJ, Tang SY, Gupta MC. Contrast-enhanced microCT evaluation of degeneration following partial and full width injuries to the mouse lumbar intervertebral disc. *Sci Rep-UK*. 2022;12:15555.
- Li D, Yang H, Huang Y, Wu Y, Sun T, Li X. Lumbar intervertebral disc puncture under C-arm fluoroscopy: a new rat model of lumbar intervertebral disc degeneration. *Exp Anim Tokyo*. 2014;63:227-234.
- Zhang L, du G, Teng B, et al. Vascular anatomy-based localization of intervertebral discs assisting needle puncture for constructing a mouse model of mechanical injury-induced lumbar intervertebral disc degeneration. *Biochem Biophys Res Commun*. 2022;634:196-202.
- Kolset SO, Pejler G. Serglycin: a structural and functional chameleon with wide impact on immune cells. *J Immunol*. 2011;187:4927-4933.
- Olmarker K. Puncture of a lumbar intervertebral disc induces changes in spontaneous pain behavior: an experimental study in rats. *Spine*. 2008;33:850-855.
- Papir-Kricheli D, Frey J, Laufer R, et al. Behavioural effects of receptor-specific substance P agonists. *Pain*. 1987;31:263-276.
- Kitamura Y, Kitagawa K, Fujitani Y, et al. The 5-HT1A receptor full agonist, 8-OH-DPAT inhibits ACTH-induced 5-HT2A receptor

- hyperfunction in rats: involvement of 5-HT1A receptors in the DOI-induced wet-dog shakes in ACTH-treated rats. *Biol Pharm Bull.* 2007;30:117-120.
16. Boyd DF, Allen EK, Randolph AG, et al. Exuberant fibroblast activity compromises lung function via ADAMTS4. *Nature.* 2020;587:466-471.
 17. Kazezian Z, Li Z, Alini M, Grad S, Pandit A. Injectable hyaluronic acid down-regulates interferon signaling molecules, IGFBP3 and IFIT3 in the bovine intervertebral disc. *Acta Biomater.* 2017;52:118-129.
 18. Studer RK, Vo N, Sowa G, Ondeck C, Kang J. Human nucleus pulposus cells react to IL-6: independent actions and amplification of response to IL-1 and TNF-alpha. *Spine.* 2011;36:593-599.
 19. Palmer A, Epton S, Crawley E, et al. Expression of p16 within myenteric neurons of the aged colon: a potential marker of declining function. *Front Neurosci-Switz.* 2021;15:747067.
 20. Lopez-Dominguez JA, Rodriguez-Lopez S, Ahumada-Castro U, et al. Cdkn1a transcript variant 2 is a marker of aging and cellular senescence. *Ageing (Albany, NY).* 2021;13:13380-13392.
 21. Balague F, Mannion AF, Pellise F, Cedraschi C. Non-specific low back pain. *Lancet.* 2012;379:482-491.
 22. Shi C, Das V, Li X, et al. Development of an in vivo mouse model of discogenic low back pain. *J Cell Physiol.* 2018;233:6589-6602.
 23. Song J, Wang HL, Song KH, et al. CircularRNA_104670 plays a critical role in intervertebral disc degeneration by functioning as a ceRNA. *Exp Mol Med.* 2018;50:1-12.
 24. Lawson L, Harfe BD. Notochord to nucleus pulposus transition. *Curr Osteoporos Rep.* 2015;13:336-341.
 25. Dowdell J, Erwin M, Choma T, Vaccaro A, Iatridis J, Cho SK. Intervertebral disk degeneration and repair. *Neurosurgery.* 2017;80:S46-S54.
 26. Liang H, Luo R, Li G, Zhang W, Song Y, Yang C. The proteolysis of ECM in intervertebral disc degeneration. *Int J Mol Sci.* 2022;23(3):1715.
 27. Li Z, Cai F, Tang J, et al. Oxygen metabolism-balanced engineered hydrogel microspheres promote the regeneration of the nucleus pulposus by inhibiting acid-sensitive complexes. *Bioact Mater.* 2023;24:346-360.
 28. Bian J, Cai F, Chen H, et al. Modulation of local overactive inflammation via injectable hydrogel microspheres. *Nano Lett.* 2021;21:2690-2698.
 29. Risbud MV, Shapiro IM. Role of cytokines in intervertebral disc degeneration: pain and disc content. *Nat Rev Rheumatol.* 2014;10:44-56.
 30. Sakahira H, Enari M, Nagata S. Cleavage of CAD inhibitor in CAD activation and DNA degradation during apoptosis. *Nature.* 1998;391:96-99.
 31. Lan T, Shiyu-Hu, Shen Z, Yan B, Chen J. New insights into the interplay between miRNAs and autophagy in the aging of intervertebral discs. *Ageing Res Rev.* 2021;65:101227.
 32. Zhou C, Yao S, Fu F, et al. Morroniside attenuates nucleus pulposus cell senescence to alleviate intervertebral disc degeneration via inhibiting ROS-Hippo-p53 pathway. *Front Pharmacol.* 2022;13:942435.
 33. Han Y, Zhou CM, Shen H, et al. Attenuation of ataxia telangiectasia mutated signalling mitigates age-associated intervertebral disc degeneration. *Ageing Cell.* 2020;19:e13162.
 34. Novais EJ, Diekman BO, Shapiro IM, Risbud MV. p16(Ink4a) deletion in cells of the intervertebral disc affects their matrix homeostasis and senescence associated secretory phenotype without altering onset of senescence. *Matrix Biol.* 2019;82:54-70.
 35. Munoz-Espin D, Serrano M. Cellular senescence: from physiology to pathology. *Nat Rev Mol Cell Biol.* 2014;15:482-496.
 36. Millecamps M, Tagerian M, Naso L, Sage HE, Stone LS. Lumbar intervertebral disc degeneration associated with axial and radiating low back pain in ageing SPARC-null mice. *Pain.* 2012;153:1167-1179.
 37. Millecamps M, Czerminski JT, Mathieu AP, Stone LS. Behavioral signs of axial low back pain and motor impairment correlate with the severity of intervertebral disc degeneration in a mouse model. *Spine J.* 2015;15:2524-2537.
 38. Nilsson E, Nakamae T, Olmarker K. Pain behavior changes following disc puncture relate to nucleus pulposus rather than to the disc injury per se: an experimental study in rats. *Open Orthop J.* 2011;5:72-77.
 39. Schellhas KP, Pollei SR, Gundry CR, Heithoff KB. Lumbar disc high-intensity zone. Correlation of magnetic resonance imaging and discography. *Spine.* 1996;21:79-86.
 40. Muralidharan A, Park TSW, Mackie JT, et al. Establishment and characterization of a novel rat model of mechanical low back pain using behavioral, pharmacologic and histologic methods. *Front Pharmacol.* 2017;8:493.
 41. Kerr GJ, McCann MR, Branch JK, et al. C57BL/6 mice are resistant to joint degeneration induced by whole-body vibration. *Osteoarthr Cartilage.* 2017;25:421-425.
 42. Yrjama M, Vanharanta H. Bony vibration stimulation: a new, non-invasive method for examining intradiscal pain. *Eur Spine J.* 1994;3:233-235.
 43. Patterson JC, Childs GV. Nerve growth factor in the anterior pituitary: regulation of secretion. *Endocrinology.* 1994;135:1697-1704.

SUPPORTING INFORMATION

Additional supporting information can be found online in the Supporting Information section at the end of this article.

How to cite this article: Huang Y, Lei L, Zhu J, et al. Pain behavior and phenotype in a modified anterior lumbar disc puncture mouse model. *JOR Spine.* 2024;7(1):e1284. doi:[10.1002/jsp2.1284](https://doi.org/10.1002/jsp2.1284)